Journal of Metals, Materials and Minerals, 35(3), e2264, 2025

Green-synthesized yttrium-doped cerium oxide nanoparticles: A promising optical material

Sasmita SARANGI[1], Nibedita NAYAK[1], Binita NANDA[2], and Tapas Ranjan SAHOO[1,*]

[1] *Department of Chemistry, School of Applied Sciences, KIIT deemed to be University, Bhubaneswar 24, Odisha, India*
[2] *Department of Chemistry, Faculty of Engineering and Technology (ITER), Siksha 'O' Anusandhan (Deemed to be University), Bhubaneswar, 751030, Odisha, India*

***Corresponding author e-mail**: trsahoofch@kiit.ac.in

Received date:
25 December 2024
Revised date:
24 April 2025
Accepted date:
10 June 2025

Keywords:
Y-doped CeO_2;
Nanoparticles;
Green synthesis;
Acacia concinna;
Optical properties

Abstract

This study examines the green production, characterization, and optical properties of yttrium-doped cerium dioxide (CeO_2) nanoparticles. A green approach was adopted using *Acacia concinna* fruit extract as a surfactant and stabilizing agent. Their structural, morphological, and physicochemical properties were characterized using different analytical techniques, like XRD, FE-SEM, FTIR, PL, Raman, and UV-Visible Spectroscopy. The XRD study validated the structure of the cubic fluorite-type structure of CeO_2 nanoparticles, with the average crystallite size ranging between 7 nm and 15 nm. Raman spectroscopy validated this structure with the F_2g band observed at 463 cm^{-1}. FESEM images showed irregular spherical morphologies with grain sizes in the range of 50 nm to 60 nm. The CeO_2 nanoparticles exhibited a prominent absorption peak at 345 nm in the UV-Visible spectrum, signifying the presence of Ce-O bonding. An increase in the Y-doping concentration in the CeO_2 lattice shifted the bandgap energy from 2.9 eV to 3.3 eV, as is evident from the Tauc plot. The PL spectra of yttrium-doped CeO_2 nanoparticles exhibited a prominent emission peak at 468 nm, attributed to oxygen vacancies in the lattice. The yttrium-doped CeO_2 nanoparticles exhibited strong visible light absorption and photoluminescence emission, which make them potential candidates for different optical applications.

1. Introduction

Nanotechnology has emerged as a cutting-edge subject that uses the special qualities of materials at the nanoscale to create novel solutions for a range of sectors, including environmental sciences, healthcare, and energy [1,2]. The outstanding physical and chemical properties of nanomaterials, particularly nanoparticles, distinguish particles beyond their substitutes in bulk [3,4]. These differences open new pathways for enhancing optical [5], catalytic [6], and electronic properties [7], making nanotechnology a promising approach for addressing modern scientific challenges [8,9]. Among various types of nanomaterials, nanoparticles synthesized from rare-earth metals have attracted considerable interest due to their distinct optical [10], magnetic [11], and electronic properties [12]. Nowadays, rare-earth (RE)-doped binary and ternary fluoride nanoparticles are the most sought-after phosphor materials because of their promise for a variety of photonic and biphotonic uses. Elements of rare earth, such as cerium and yttrium, possess unique electronic configurations that contribute to their utility in advanced technological applications [13]. Cerium, in particular, stands out for its versatility and functionality in fields ranging from catalysis to optoelectronics [14,15]. Cerium dioxide (CeO_2) nanoparticles, or nanoceria, are of particular importance due to their high oxygen storage capacity [16,17], redox behavior [18,19], and UV-shielding capabilities [20]. These properties make CeO_2 nanoparticles highly suitable for applications in catalysis [21], biomedical sciences [22], and optical devices [23,24]. In recent years, the doping of cerium dioxide nanoparticles with rare-earth elements, such as yttrium [25,26], has emerged as an effective method to enhance their inherent properties and expand their functionality [27]. Yttrium-doped cerium dioxide (CeO_2) nanoparticles offer improvements in optical and electronic behaviour, which are desirable for applications in optics and photonics [28,29]. The majority of cerium and yttrium elements have been examined in detail, independently or in combination, for the creation of fuel cell nanocrystalline bodies [30], catalytic [31], ceramics [32,33], and optical applications [34]. Like lanthanides, yttrium and scandium are rare earth elements. In addition to lanthanides, cerium, gadolinium (Gd), and lutetium (Lu) are the most closely linked to the d-block transition metals. Because valence electrons are present in the 5d orbitals of the Ce, Gd, and Lu atoms, this final association is valid [35]. In addition to the more prevalent +3 state for rare earth elements like Y, Ce atoms can also take up the +4-oxidation state in a range of ways [36]. Strong evidence has associated the antioxidant with reversible transitions between the Ce^{3+} and Ce^{4+} oxidation levels of ceria nanoparticles [37]. Yttrium's addition to CeO_2 influences the bandgap, stabilizes the structure, and enhances the photoluminescence of the nanoparticles [38,39]. The introduction of Y^{3+} ions into the CeO_2 lattice, substituting for Ce^{4+} ions, results in a local positive charge imbalance due to the disparity in oxidation states Specifically, each Y^{3+} ion carries one unit less positive charge compared to Ce^{4+}. To maintain overall charge neutrality in the crystal, this charge deficiency is compensated by the formation of oxygen vacancies. For every two Y^{3+} ions substituting two Ce^{4+} ions, one O^{2-} anion is removed from the lattice, resulting in the creation of an oxygen vacancy. These modified optical properties make CeO_2 nanoparticles highly applicable in areas such as UV filtering

[40], photocatalysis [41], and energy-efficient lighting [42]. Y-doped CeO_2 nanoparticles' luminescence properties are very remarkable [43]. The nanoparticles' long-term stability is demonstrated through a combination of optical characterization and structural investigation. Measurements of photoluminescence (PL) showed no changes in intensity or peak position over time, indicating constant optical characteristics. The absence of new absorbance peaks indicates no chemical transformations or degradation processes, which proves long term stability of these nanoparticles.

By altering the electronic structure and defect chemistry, yttrium doping alters the optical band gap of cerium dioxide, resulting in enhanced absorption and emission characteristics [44]. These properties are beneficial in designing materials for high-performance optical devices [45]. As a result, the CeO_2 lattice displays structural changes upon the addition of yttrium ions, increasing stability and improving the control of particle size and morphology [46,47]. This control is particularly advantageous when nanoparticles are synthesized using environmentally friendly, or "green," synthesis approaches, which utilize natural stabilizing agents [48]. This study aims to synthesize yttrium-doped cerium dioxide nanoparticles through a green synthesis route utilizing acacia concinna fruit extract as a stabilizing agent [49]. This method provides an eco-friendly alternative to conventional chemical methods, mitigating the detrimental impacts of nanoparticle production on the environment. The created nanoparticles are thoroughly characterized to assess their structural, morphological, and optical properties, with a focus on their potential applications as optical materials [50]. This study effectively illustrated the environmentally friendly synthesis of yttrium-doped cerium oxide (Y-doped CeO_2) nanoparticles utilizing the sol-gel method by using extract of Acacia concinna fruit [51]. This sustainable strategy provides a sustainable alternative to conventional chemical techniques, reducing the usage of hazardous chemicals and reducing environmental effects. Optical properties of the synthesized Y-doped CeO_2 nanoparticles were investigated through photoluminescence studies and energy band gap analysis [52]. The results revealed the promising potential of these nanoparticles in optical applications. The observed luminescence properties can be attributed to the synergistic effect of yttrium doping, which influences the electronic structure and defect states within the CeO_2 lattice [53]. To maximize the production procedure and investigate the possible uses of these nanoparticles in many domains, more investigation is required, such as in catalysis, sensors, and biomedicine. By delving deeper into their fundamental properties and tailoring their characteristics, we can unlock their full potential and contribute to the development of innovative technologies.

2. Experimental

2.1 Materials synthesis

The yttrium(III) nitrate hexahydrate [$Y(NO_3)_3{\cdot}6H_2O$] and ammonium cerium (IV) nitrate [$(NH_4)_2Ce(NO_3)_6$] salts purchased from S.R.L. chemicals were utilized in the synthesis of CeO_2 and Y-doped CeO_2 NPs. The sol-gel method was used in a standard procedure to generate pure and 1%, 3%, and 5% Y-doped CeO_2 NPs. The Acacia Concinna fruits were gathered from the marketplace, sun-dried, unseeded, and their pericarp thoroughly ground in a mixer to create a fine powder. 200 mL of double-distilled water was combined with 20 g of powdered Acacia Concinna pericarp, and the mixture was agitated for 2 h at 60°C. It was cooled, filtered, and kept for future research at 4°C. 20 mL of Acacia Concinna fruit extract was initially obtained and mixed with a magnetic stirrer at 60°C for 30 min at 450 rpm in order to create cerium oxide nanoparticles (CeO_2 NPs). The extract was then heated to 80°C while being constantly stirred at 450 rpm until a jelly-like mass formed, after which 4 g of ammonium cerium (IV) nitrate was added. This gel was oven-dried at 80 to 90 degrees Celsius and then calcined in a muffle furnace for two hours at 400 degrees Celsius to yield the white powder known as CeO_2 nanoparticles. To create Y-doped CeO_2 nanoparticles, these metal nitrates were also added to the fruit extract in stoichiometric ratios. The mixtures were then heated and calcined in the same way. The final product was generated by calcining the gels once they dried for two hours at 400°C in a muffle furnace.

2.2 Instrumentation and methodology

Several analytical methods were used to determine the form, structure, content, and other physicochemical characteristics of the Y-doped CeO_2 nanoparticles. The properties of the samples have been analysed through the application of X-ray diffraction (XRD), Field emission scanning electron microscopy (FESEM), Raman spectroscopy, and Fourier transform infrared spectroscopy (FTIR) techniques. A Bruker advanced X-ray diffractometer was used for phase identification of both nano-particles that were subjected to CuKa radiation (k= 0.154184 nm) at 10 to 100. The samples' morphology was evaluated with ZEISS FESEM. To ascertain the origin and purity of synthesized materials, FTIR spectra were obtained in ATR mode using a Bruker ALPHA II FTIR spectrophotometer. To determine the vibrational mode of the NPs, a Renishaw UK spectrometer with a red diode laser (633) performed Raman spectroscopy. For the UV spectrum, a JASCO-V 770 spectro-photometer was used.

3. Results and discussions

3.1 X-ray diffraction (XRD)

One method for figuring out a material's crystal structure and phase purity is XRD. The XRD spectra of Y-doped CeO_2 and CeO_2 nanoparticles are demonstrated in Figure 1(a), illustrating the nano-crystalline structure of the materials. For both pure and Y-doped CeO_2 NPs, all diffraction peaks indexed to crystal planes (111), (200), (220), (311), (222), (400), (331), (420), (442), and (511), which correspond to the cubic fluorite structure of CeO_2 with the Fm-3m space group. The absence of additional peaks implies that the cubic phase is a single phase found in pristine and Y-doped CeO_2 NPs. Additionally, as exhibited in Figure 1(b), the major peak's (111) location shifted towards lower angles, ensuring the effective doping of yttrium ions into the CeO_2 crystal lattice. When crystallites are smaller, the surface-to-volume ratio increases. This means that more atoms are located on the surface or near the surface, which can result in a shift to higher angles. When Ce^{4+} ions (1.01 Å) are replaced by Y^{3+} ions (0.96 Å), lattice contraction and deformation contribute to the displacement of the peak. Figure 1(c) demonstrates that as the Y doping concentration rose from 0% to 5%, lattice parameter and crystallite size values

were shown. This might perhaps be ascribed to the lattice contraction resulting from the substitution of bigger Ce^{4+} ions with smaller Y^{3+} ions. The absence of additional phases, as well as changes in lattice parameter and crystallite size, indicates that Y ions were successfully doped into the CeO_2 host matrix.

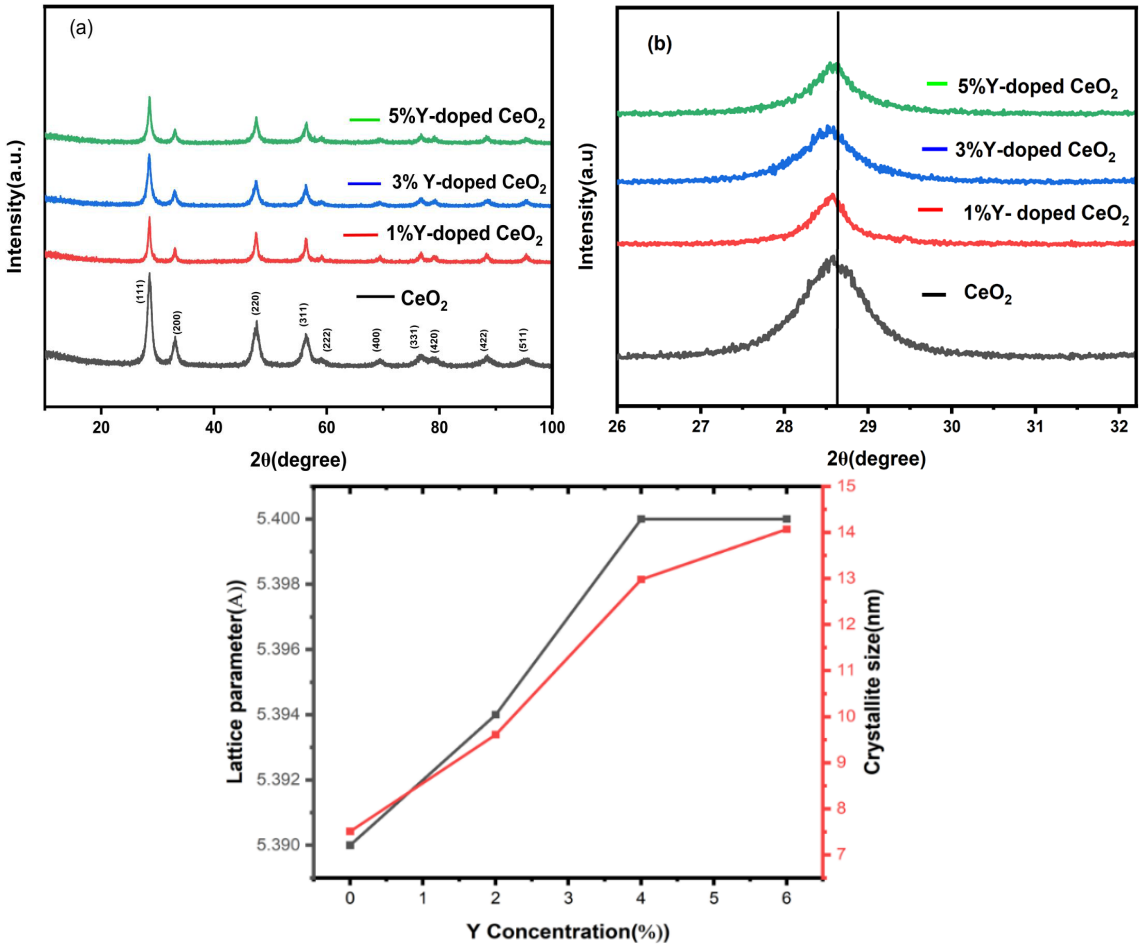

Figure 1. (a) XRD pattern of CeO_2 NPs and Y-doped CeO_2 NPs, (b) Shift in the (111) peak due to doping of Y, (c) Variation of crystallite size and lattice parameter of CeO_2 NPs with Y dopant concentration.

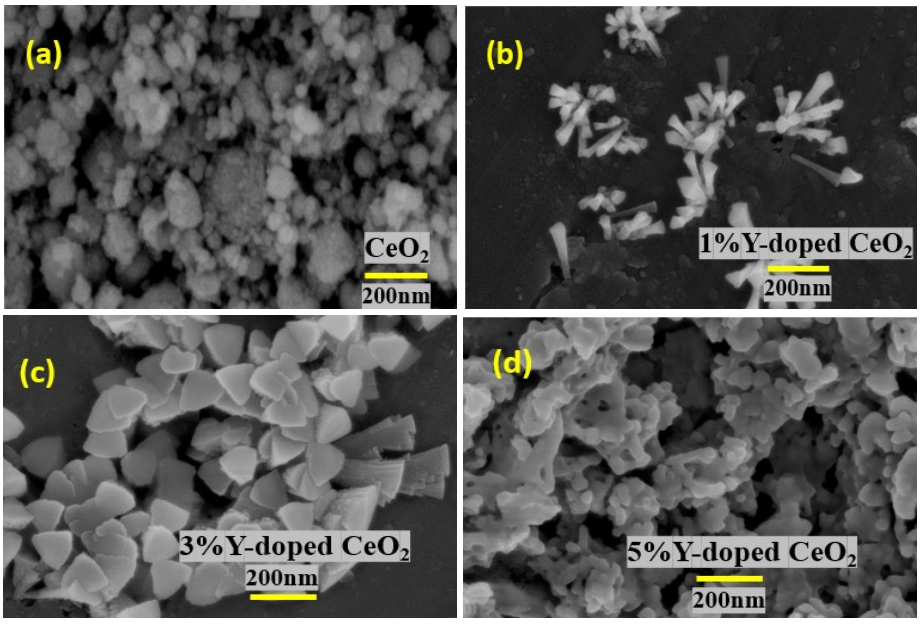

Figure 2. FE-SEM images of (a) CeO_2 NPs, (b) 1%, (c) 3%, and (d) 5% Y-doped CeO_2 NPs.

3.2 Field emission scanning electron microscope (FESEM)

The images highlight the morphology of pure and yttrium-doped CeO_2 nanoparticles as highlighted by FESEM. Figure 2(a) exhibits pure CeO_2 nanoparticles. They appear to have a spherical shape with a relatively smooth surface. Figure 2(b) shows 1% yttrium-doped CeO_2 nanoparticles. The morphology has changed to a more needle-like or rod-like structure compared to the pure CeO_2. FESEM images of yttrium-doped cerium dioxide nanoparticles reveal a morphological shift from spherical to needle-like structures, likely due to anisotropic crystal formation. This shift is attributed to localized lattice strain and altered surface energy dynamics. Y-doping selectively adsorbs on specific crystal facets, promoting anisotropic crystal development and allowing higher development in other directions. This phenomenon is known as selective facet stabilization Figure 2(c) shows 3% yttrium-doped CeO_2 nanoparticles. The morphology is similar to the 1% doped sample, with needle-like structures. Figure 2(d) shows 5% yttrium-doped CeO_2 nanoparticles. The morphology is again similar to the lower doped samples, with needle-like structures. Thus, it seems that yttrium doping induces a change in the morphology of CeO_2 nanoparticles from spherical to needle-like. The material's optical characteristics may be affected by this structural change. This change in morphology may impact the material's optical properties, such as its surface area and catalytic activity. Using ImageJ software, the particles' grain size was found to be between 40 nm and 56 nm. Additionally, the EDX spectra verify that Ce and Y are present in the doped nanoparticles.

3.3 Energy dispersive x-ray analysis (EDX)

Figure 3(a) shows EDX spectra of 5% yttrium-doped CeO_2 nanoparticles. Energy dispersive x-ray analysis (EDX) provides quantitative information on the elemental composition of Y-doped CeO_2 nanoparticles. In this analysis, peaks corresponding to cerium (Ce), oxygen (O), and yttrium (Y) confirm the successful integration of yttrium ions into the CeO_2 lattice. The intensity and presence of these peaks can be used to quantify the doping concentration of yttrium. The absence of additional peaks indicates that the synthesis yielded pure doped CeO_2 nanoparticles without significant contamination.

Elemental mapping: Figure 3(b) shows elemental mapping of 5% yttrium-doped CeO_2 nanoparticles. Elemental mapping, typically performed alongside EDX in scanning electron microscopy (SEM) or transmission electron microscopy (TEM), visually demonstrates the distribution of elements within the nanoparticles. The spectrum reveals the presence of oxygen, cerium, and yttrium. Maps of Ce, Y, and O show the uniform distribution of yttrium within the CeO_2 matrix, indicating homogeneous doping. Uniform yttrium distribution is critical as it ensures consistent optical and structural properties throughout the nanoparticle samples. Elemental mapping imagery also reveals any clustering or segregation of yttrium, which could affect the material's properties. Together, EDX and elemental mapping confirm successful yttrium incorporation and uniform distribution in CeO_2 nanoparticles, essential for maintaining desired optical and structural characteristics.

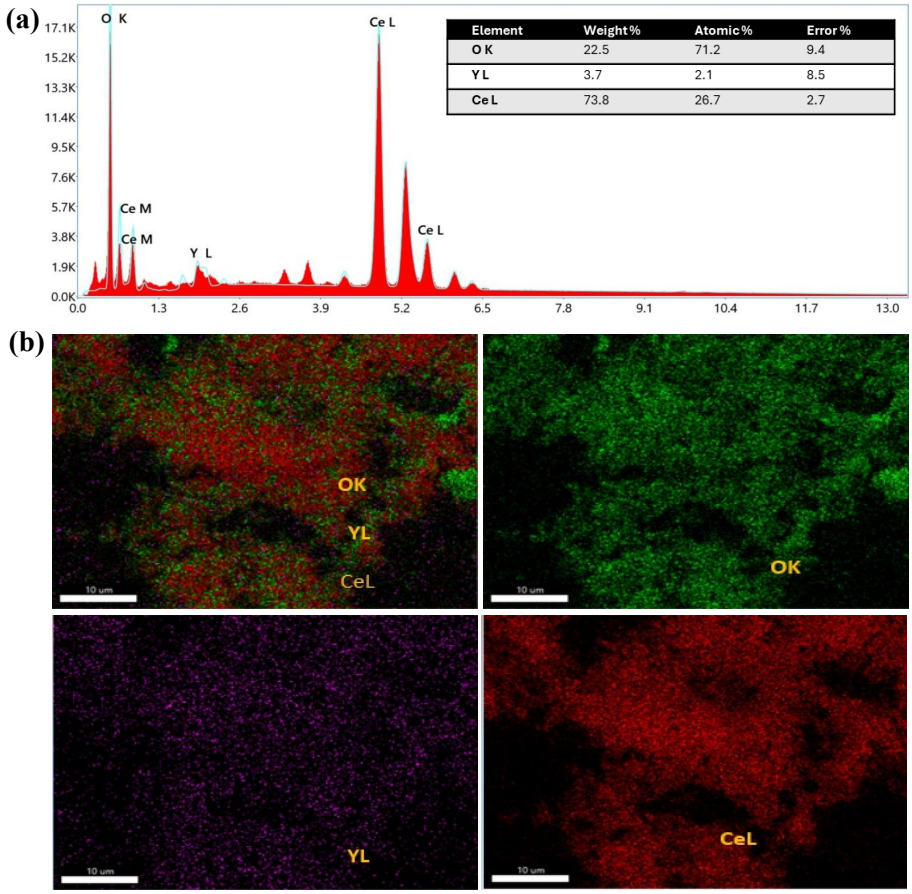

Figure 3. (a) EDX of 5 % Y-doped CeO_2 NPs, and (b) Elemental composition found using EDAX of 5 % Y-doped CeO_2 NPs.

3.4 Raman spectroscopy

We can examine the lattice defects with the aid of Raman analysis. Figure 3(a) depicts the Raman spectra of pure CeO_2 NPs, 1%, 3%, and 5% Y-doped CeO_2 NPs, and Figure 3(b) shows changes in the F_{2g} peak generated due to Y doping. This method is non-destructive. At room temperature, Raman spectroscopy of CeO_2 and Y-doped CeO_2 NPs was obtained. Consequently, of the symmetric stretching of the Ce–O bond, the Raman active vibrational mode at 462.58 cm^{-1} is the peak of maximal intensity for the triply produced F_{2g} excitation mode. When compared to the Raman peak of bulk CeO_2, there is a significant shift toward a greater wavenumber region that is frequently linked to the formation of oxygen vacancy in the system. The Y ions, in addition to the CeO_2 lattice, caused a blue shift in the F2g Raman active mode, which might be enhanced with the development of additional oxygen vacancies as a result of the effects of the dopant.

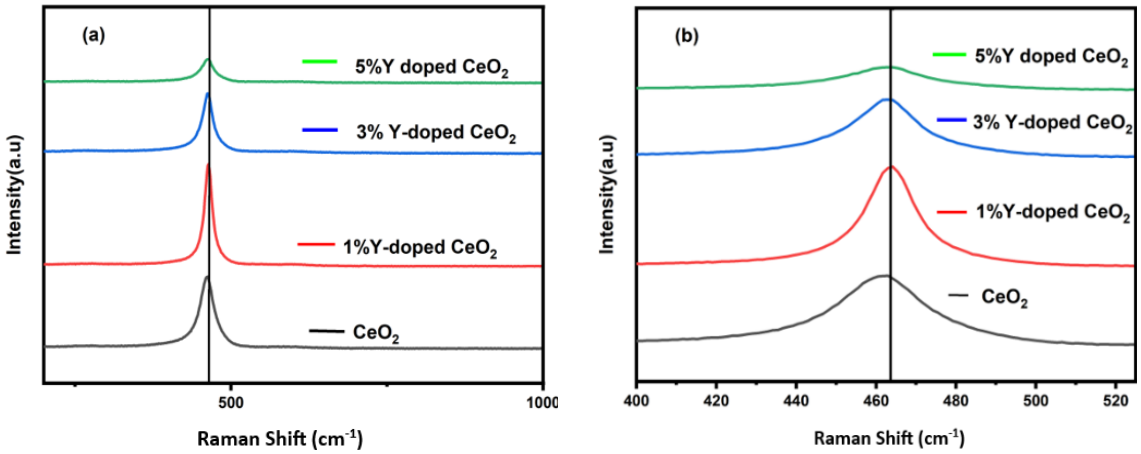

Figure 4. (a) Raman spectra of CeO_2 NPs, 1%, 3%, and 5% Y-doped CeO_2NPs. (b) Shift in the F_{2g} peak due to doping of Y.

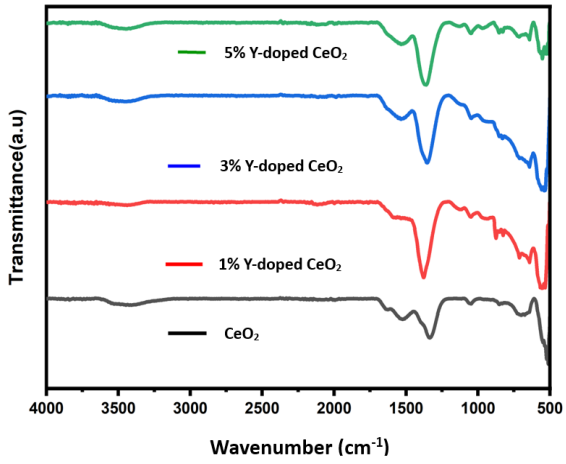

Figure 5. FTIR spectra of CeO2 NPs, 1%, 3%, and 5% Y-doped CeO2 NPs.

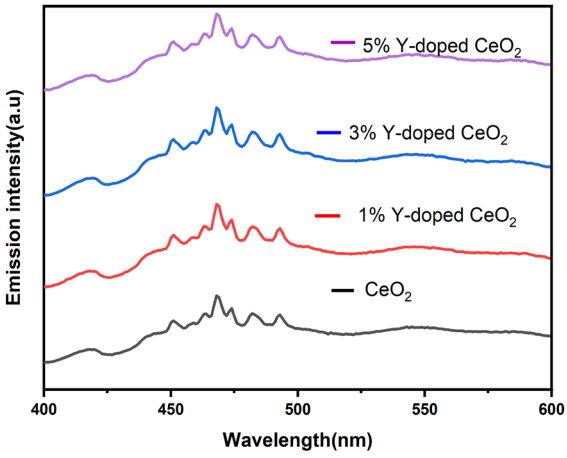

Figure 6. Photoluminescence spectra of (a) CeO_2 NPs, (b) 1%, (c) 3%, (d) 5% Y-doped CeO_2 NPs.

3.5 Fourier transform infrared spectroscopy (FTIR)

FTIR spectra were obtained for CeO_2 NPs and Y-doped CeO_2 NPs in the 500 cm^{-1} to 4000 cm^{-1} range. The existence of functional groups was investigated using FTIR analysis. The different absorption peaks and bands of Y-doped CeO_2 NPs are shown in Figure 5. The symmetric stretching of O_2^- ions in the structure, which preserves symmetry in the host lattice, is the cause of the band seen around 500 cm^{-1}, which corresponds to the stretching vibrations of the O–Ce–O bond. The stretching vibrations of carbon dioxide species are responsible for the peaks, which are roughly situated at 876 cm^{-1} and 1050 cm^{-1}, respectively. The peak at 641 cm^{-1} may be due to vibrations caused by Ce–O–Y bonding or interactions between dopant ions and oxygen vacancies in the CeO_2 lattice. The nitrate precursor is responsible for the prominent peak that is observed at 1345 cm^{-1}. The O–H stretching resulting from the process of water molecules adhering in the samples causes the broad peak at 3425 cm^{-1}.

3.6 Optical properties

3.6.1 PL spectral analysis

Photoluminescence Spectra (PL) for (a) CeO_2 NPs, (b) 1%, (c) 3%, and (d) 5% Y-doped CeO_2 NPs are shown in Figure 7. Using photoluminescence (PL) spectroscopy, the electrical structure of the produced CeO_2 nanoparticles was investigated. PL is the most advanced method for determining the material's optical characteristics without destroying the sample when compared to other optical characterization tools. Photoluminescence emission in CeO_2 nano-particles is attributed to defect states like oxygen vacancies or Y-induced lattice distortions. Y^{3+} dopant ions can produce localized energy levels, promoting emission.

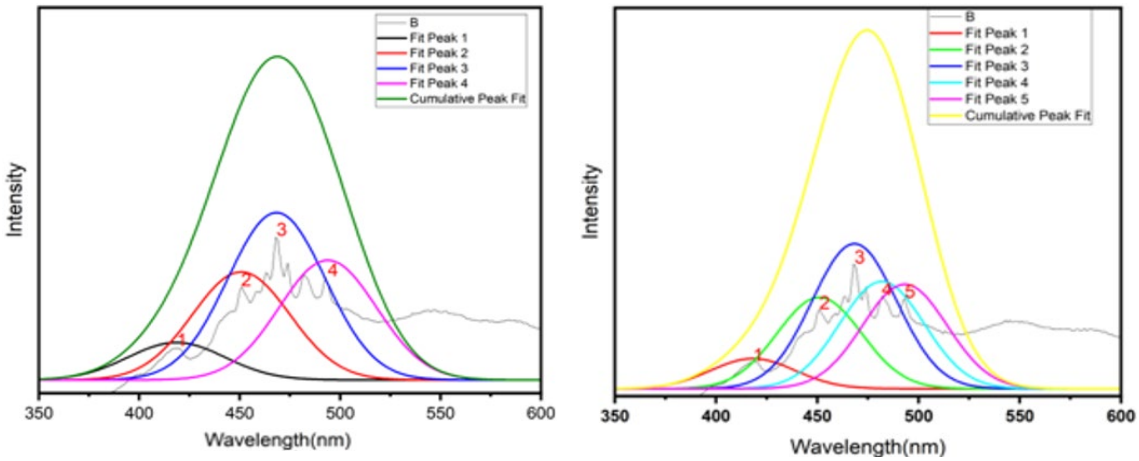

Figure 7. Deconvolution peak of CeO_2, and 5% of Y-doped CeO_2 NPs.

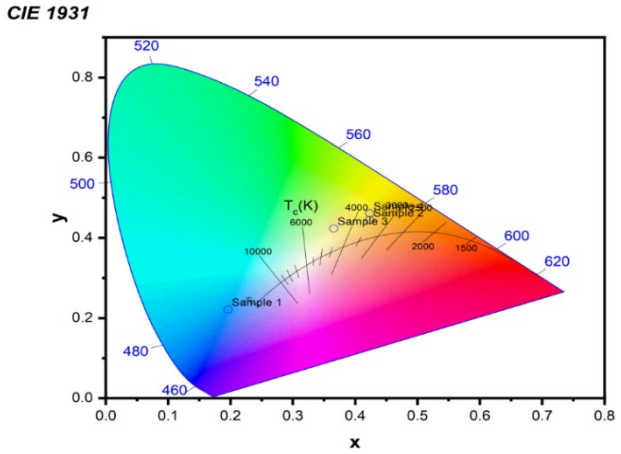

Figure 8. Chromaticity diagram of Y-doped CeO_2 NPs.

Blue light (~468 nm) is released when electrons drop to these vacancy levels from the conduction band or trap states. Ce^{3+} transitions, oxygen vacancy states, and direct band-to-band recombination contribute to blue emission. Quantum Yield measurements were done for CeO_2 and 5% Y-doped CeO_2. But the quantum yield (QY) % obtained were very low. The QY for CeO_2 was 0.17% and for 5% Y-doped CeO_2 was 0.07% only.

Under 325 nm excitation, the CeO_2 nanoparticles' acquired PL spectra in the 400 nm to 600 nm wavelength range were captured. A fine UV emission can be seen at 358 nm (3.47 eV) in the CeO_2 nanoparticles' PL spectra, whereas the blue area shows four visible emission peaks: 452 nm (2.74 eV), 469 nm (2.64 eV), 483 nm (2.57 eV), and 493 nm (2.52 eV). Strong green emission was also detected at 574 nm (2.16 eV) in addition to this. The relative oxygen vacancies (surface defects) of CeO_2 nanoparticles are the source of the emission band seen in the wavelength range of 358 nm to 574 nm. It might result from variations in particle size. The movement of charge carriers from the CeO_2 nanoparticles' 4f conduction band (Ce) to their 2p valence band (O) can also be used to explain the relative oxygen vacancies. Figure 8 illustrates the deconvolution peaks of CeO_2 and 5% Y-doped CeO_2 nanoparticles, which roughly correspond to the impact of yttrium doping on the electrical structure of cerium oxide. The various binding energies linked to the Ce^{3+} and Ce^{4+} oxidation states are represented by these peaks.

3.6.2 Chromaticity coordinates

The chromaticity diagram of Y-doped CeO_2 NPs is displayed in Figure 9. The chromaticity coordinates, which indicate the physical colour of light, can be used to describe its spectrum. Nonetheless, in certain applications, it is crucial to understand how the human eye would interpret light from a specific spectrum. The instruments that offer a mathematical explanation of colour perception for a particular spectrum are CIE colour spaces. Commission Internationale de l'Éclairage, or CIE for short, is the French name of the International Commission on Illumination, which created the methods. Cone cells are a particular type of light-sensitive retinal cell that is responsible for colour vision. Cone cells come in three varieties, each of which is sensitive to red, green, and blue light. They are all distinguished by their peak sensitivity wavelengths. The so-called colour matching functions were created based on the average cone cell density in the human retina as well as the sensitivity spectra of each type of cone cell. A standard observer is a specific collection of functions. A number of distinct standards are observed. The method's concept included separating brightness and chromaticity. The brightness information would be included in the Y tristimulus value thanks to the development of the colour matching routines. A chromaticity diagram can show the colour as a point once the coordinates have been determined. The functions for matching colours are displayed in Figure 7. The CIE 1931 chromaticity diagram of Y-doped CeO_2 NPs is shown in Figure 8.

3.6.3 UV-Visible studies

The band gap values of the synthesized pure CeO_2 and yttrium-doped CeO_2 nanoparticles were estimated from UV–Vis spectroscopy. The bandgap (E_g) value of pure CeO_2 is around 3.2 eV, and yttrium-doped CeO_2 is 2.9 eV, where the corresponding wavelength exists in the visible region. Figure 9(a) displays the UV-Vis absorption spectra of Y-doped CeO_2 and CeO_2 nanoparticles, and Figure 9(b) demonstrates the TAUC plot of CeO_2 and Y-doped CeO_2NPs. The CeO_2 nanoparticles have a prominent absorption peak at 345 nm. Using the TAUC relation, the band gap energies of the synthesized samples were determined as follows:

$$(\alpha h\nu)^2 = A(h\nu - E_g) \quad (1)$$

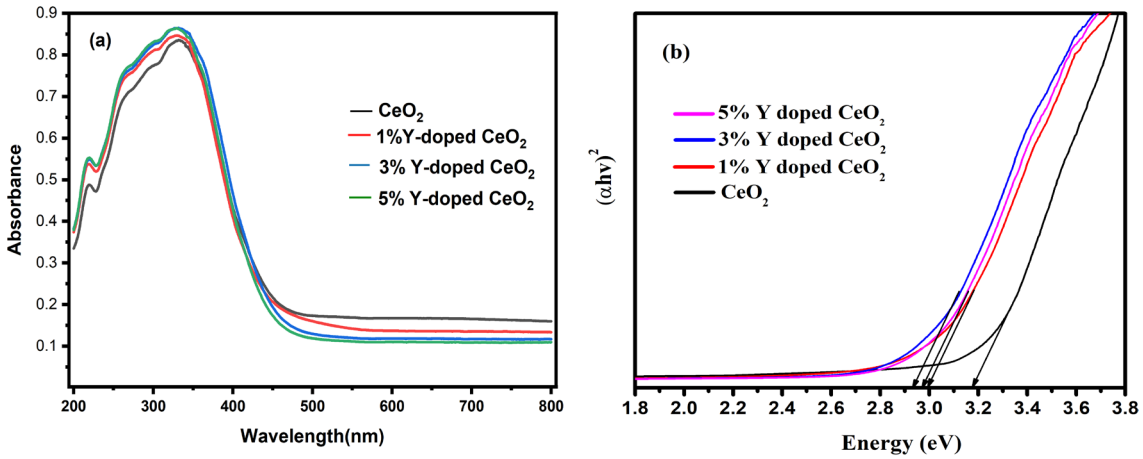

Figure 9. (a) UV-VIS spectra of CeO_2 NPs, 1%, 3% and 5% Y-doped CeO_2 NPs, and (b) TAUC plot of CeO_2, 1%, 3%, and 5% Y-doped CeO_2 NPs.

Where 'α' is the absorption coefficient, 'hν' is photon energy, 'A' is a constant, and 'E_g' is the optical band gap energy of Y-doped CeO_2 NPs. Plotting $(\alpha h\nu)^2$ versus hν and extrapolating the straight-line portion of this plot to the energy axis will produce the optical band gap energy of the nanoparticles. As the concentration of Y was raised from 1% to 5% doping, the bandgap energy decreased from 3.2 eV to 2.9 eV. The decrease in the band gap energy may be attributed to the formation of defects in the crystal lattice of CeO_2 NPs. .

4. Conclusions

Green synthesis of yttrium-doped cerium oxide (Y-CeO_2) nanoparticles, which uses extract from Acacia concinna as a natural stabilizing agent and surfactant, offers an environmentally responsible method of creating cutting-edge optical materials. Structural and morphological analyses confirmed the successful incorporation of yttrium into the CeO_2 lattice, resulting in nanoparticles with a cubic fluorite structure, average crystallite sizes of 7 nm to 15 nm, and distinct surface characteristics. Optical characterization revealed a tunable band gap with prominent UV-visible absorption and a photo-luminescent peak at 468 nm, linked to oxygen vacancies within the structure. These findings highlight the promising optical properties of Y-doped CeO_2 nanoparticles. The green synthesis method underscores a sustainable pathway for producing useful nanoparticles with enhanced performance and reduced environmental impact. Our results demonstrate that Y-doped CeO_2 nanoparticles exhibit superior optical characteristics and luminescence properties.

Acknowledgements

Authors are thankful to the KIIT Deemed to be University for providing the platform and support to carry out this work.

References

[1] J. Gidiagba, C. Daraojimba, K. A. Ofonagoro, N. L. Eyo-Udo, B. Egbokhaebho, O. A. Ogunjobi, and A. Banso, "Economic impacts and innovations in materials science: A holistic exploration of nanotechnology and advanced materials," *Engineering Science & Technology Journal,* vol. 4, no. 3, pp. 84-100, 2023.

[2] H. S. Das, A. Basak, and S. Maity, "Materials science and nanotechnology," in *Innovations in Energy Efficient Construction Through Sustainable Materials*: IGI Global, 2025, pp. 175-206.

[3] N. Joudeh, and D. Linke, "Nanoparticle classification, physico-chemical properties, characterization, and applications: A comprehensive review for biologists," *Journal of Nanobio-technology,* vol. 20, no. 1, p. 262, 2022.

[4] P. Lakhani, D. Bhanderi, and C. K. Modi, "Nanocatalysis: recent progress, mechanistic insights, and diverse applications," *Journal of Nanoparticle Research,* vol. 26, no. 7, p. 148, 2024.

[5] M. Kapilashrami, Y. Zhang, Y.-S. Liu, A. Hagfeldt, and J. Guo, "Probing the optical property and electronic structure of TiO_2 nanomaterials for renewable energy applications," *Chemical reviews,* vol. 114, no. 19, pp. 9662-9707, 2014.

[6] A. A. Sharma, M. Rakshita, P. P. Pradhan, K. A. Durga Prasad, S. Mishra, K. Jayanthi, D. Haranath, "Efficacy of photodynamic therapy using UVB radiation-emitting novel phosphor material for non-surgical treatment of psoriasis," *Journal of Materials Research*. vol. 38, no. 10, pp. 2812-22, 2023.

[7] S. F. Ahmed, M. Mofijur, N. Rafa, A. T. Chowdhury, S. Chowdhury, M. Nahrin, A. B. M. Saiful Islam, and H. C. Ong, "Green approaches in synthesising nanomaterials for environmental nanobioremediation: Technological advancements, applications, benefits and challenges," *Environmental Research,* vol. 204, p. 111967, 2022.

[8] S. M. Rodrigues *et al.*, "Nanotechnology for sustainable food production: promising opportunities and scientific challenges," *Environmental Science: Nano,* vol. 4, no. 4, pp. 767-781, 2017.

[9] N. Baig, I. Kammakakam, and W. Falath, "Nanomaterials: A review of synthesis methods, properties, recent progress, and challenges," *Materials advances,* vol. 2, no. 6, pp. 1821-1871, 2021.

[10] S. K. Gupta, K. Sudarshan, and R. Kadam, "Optical nano-materials with focus on rare earth doped oxide: A Review," *Materials Today Communications,* vol. 27, p. 102277, 2021.

[11] S. Gai, C. Li, P. Yang, and J. Lin, "Recent progress in rare earth micro/nanocrystals: Soft chemical synthesis, luminescent

properties, and biomedical applications," *Chemical reviews,* vol. 114, no. 4, pp. 2343-2389, 2014.

[12] S. Sharma, A. Sharma, S. Sankhyan, A. Kumar, and A. K. Sharma, "Antimicrobial nanoparticles: production, mechanism of action, and applications in the food sector," in *Nanotechnology Horizons in Food ProcessEngineering*, 2023, pp. 227-284.

[13] B. Zheng, J. Fan, B. Chen, X. Qin, J. Wang, F. Wang, R. Deng, and X. Liu, "Rare-earth doping in nanostructured inorganic materials," *Chemical Reviews,* vol. 122, no. 6, pp. 5519-5603, 2022.

[14] J. Ballato, J. S. Lewis, and P. Holloway, "Display applications of rare-earth-doped materials," *MRS Bulletin,* vol. 24, no. 9, pp. 51-56, 1999.

[15] E. Kusmierek, "A CeO_2 semiconductor as a photocatalytic and photoelectrocatalytic material for the remediation of pollutants in industrial wastewater: a review," *Catalysts,* vol. 10, no. 12, p. 1435, 2020.

[16] M. Rakshita, A. Babu, K. Jayanthi, S. Bathula, K.U. Kumar, and D. Haranath, "Studies on contact angle measurements in superoleophobic aluminum hydroxide nanoflakes," *Materials Letters*, vol. 315, p. 131938, 2022.

[17] R. C. Deus, C. R. Foschini, B. Spitova, F. Moura, E. Longo, and A. Simoes, "Effect of soaking time on the photoluminescence properties of cerium oxide nanoparticles," *Ceramics International,* vol. 40, no. 1, pp. 1-9, 2014.

[18] S. N. Naidi, M. H. Harunsani, A. L. Tan, and M. M. Khan, "Green-synthesized $CeO_{(2)}$ nanoparticles for photocatalytic, antimicrobial, antioxidant and cytotoxicity activities," *Journal Mater Chem B,* vol. 9, no. 28, pp. 5599-5620, 2021.

[19] Y. Xu, "Morphological Mapping and Growth Mechanisms of Ceria Nanocrystals," UNSW Sydney, 2019.

[20] Y. Li, X. Bian, W. Wu, and H. Dong, "Synthesis, characterization, and double shielding performance for ultraviolet and short-wave blue light of ceria-based materials," *Ceramics International,* vol. 50, no. 22, pp. 48592-48599, 2024.

[21] C. Walkey, S. Das, S. Seal, J. Erlichman, K. Heckman, L. Ghibelli, E. Traversa, J. F. McGinnis, and W. T. Self, "Catalytic properties and biomedical applications of cerium oxide nanoparticles," *Environ Sci Nano,* vol. 2, no. 1, pp. 33-53, 2015.

[22] A. B. Shcherbakov, V. V. Reukov, A. V. Yakimansky, E. L. Krasnopeeva, O. S. Ivanova, A. L. Popov, and V. K. Ivanov, "CeO_2 nanoparticle-containing polymers for biomedical applications: A review," *Polymers,* vol. 13, no. 6, p. 924, 2021.

[23] S.-Y. Ahn, W.-J. Jang, J.-O. Shim, B.-H. Jeon, and H.-S. Roh, "CeO_2-based oxygen storage capacity materials in environmental and energy catalysis for carbon neutrality: Extended application and key catalytic properties," *Catalysis Reviews,* vol. 66, no. 4, pp. 1316-1399, 2024.

[24] N. J. Bassous, C. B. Garcia, and T. J. Webster, "A study of the chemistries, growth mechanisms, and antibacterial properties of cerium-and yttrium-containing nanoparticles," *ACS Biomaterials Science & Engineering,* vol. 7, no. 5, pp. 1787-1807, 2020.

[25] A. Kubiak, and M. Cegłowski, "Unraveling the impact of microwave-assisted techniques in the fabrication of yttrium-doped TiO2 photocatalyst," *Scientific Reports,* vol. 14, no. 1, p. 262, 2024.

[26] E. Zhang, Y. Bandera, A. Dickey, J. W. Kolis, and S. H. Foulger, "Enhanced radioluminescence of yttrium pyrosilicate nanoparticles via rare earth multiplex doping," *Nanoscale,* vol. 14, no. 33, pp. 12030-12037, 2022.

[27] B.-H. Chen, and B. Stephen Inbaraj, "Various physicochemical and surface properties controlling the bioactivity of cerium oxide nanoparticles," *Critical Reviews in Biotechnology,* vol. 38, no. 7, pp. 1003-1024, 2018.

[28] E. Hannachi, Y. Slimani, M. Nawaz, R. Sivakumar, Z. Trabelsi, R. Vignesh, S. Akhtar, M. A. Almessiere, A. Baykal, and G. Yasin, "Preparation of cerium and yttrium doped ZnO nanoparticles and tracking their structural, optical, and photocatalytic performances," *Journal of Rare Earths,* vol. 41, no. 5, pp. 682-688, 2023.

[29] B. Xu, Q. Zhang, S. Yuan, S. Liu, M. Zhang, and T. Ohno, "Synthesis and photocatalytic performance of yttrium-doped CeO_2 with a hollow sphere structure," *Catalysis Today,* vol. 281, pp. 135-143, 2017.

[30] M. Rakshita, A. A. Sharma, P. P. Pradhan, K. D. Prasad, M. Srinivas, and D. Haranath, "Fabrication and characterization of rare earth-free nanophosphor-based devices for solid-state lighting applications." *Materials Advances*, vol. 6, pp. 3203-3219, 2025.

[31] L. Wang, and H. Jia, "Yttrium doped cerium oxide as free radical scavenger for proton exchange membrane fuel cells," *International Journal of Hydrogen Energy,* vol. 82, pp. 265-271, 2024.

[32] B. Xu, Q. Zhang, S. Yuan, M. Zhang, and T. Ohno, "Morphology control and photocatalytic characterization of yttrium-doped hedgehog-like CeO_2," *Applied Catalysis B: Environmental,* vol. 164, pp. 120-127, 2015.

[33] M. Jamshidijam, P. Thangaraj, A. Akbari-Fakhrabadi, M. A. N. Galeano, J. Usuba, and M. R. Viswanathan, "Influence of rare earth (RE= Nd, Y, Pr and Er) doping on the micro-structural and optical properties of ceria nanostructures," *Ceramics International,* vol. 43, no. 6, pp. 5216-5222, 2017.

[34] K. Seth, "Recent progress in rare-earth metal-catalyzed sp2 and sp3 C–H functionalization to construct C–C and C–heteroelement bonds," *Organic Chemistry Frontiers,* vol. 9, no. 11, pp. 3102-3141, 2022.

[35] Y. Wang, J. Liang, C. Deng, R. Sun, P-X. Fu, B-W. Wang, S. Gao, and W. Huang, "Two-electron oxidations at a single cerium center," *Journal of the American Chemical Society,* vol. 145, no. 41, pp. 22466-22474, 2023.

[36] T. Vinodkumar, B. G. Rao, and B. M. Reddy, "Influence of isovalent and aliovalent dopants on the reactivity of cerium oxide for catalytic applications," *Catalysis Today,* vol. 253, pp. 57-64, 2015.

[37] V. Seminko, P. Maksimchuk, G. Grygorova, E. Okrushko, O. Avrunin, V. Semenets, and Y. V. Malyukin, "Mechanism and dynamics of fast redox cycling in cerium oxide nanoparticles at high oxidant concentration," *The Journal of Physical Chemistry C,* vol. 125, no. 8, pp. 4743-4749, 2021.

[38] J. Malleshappa, H. Nagabhushana, B. D. Prasad, S. Sharma, Y. Vidya, and K. Anantharaju, "Structural, photoluminescence

and thermoluminescence properties of CeO_2 nanoparticles," *Optik,* vol. 127, no. 2, pp. 855-861, 2016.

[39] R. Kırkgeçit, H. Ö. Torun, F. K. Dokan, and E. Öztürk, "Optical and electrical conductivity properties of rare earth elements (Sm, Y, La, Er) co-doped CeO_2," *Journal of Rare Earths,* vol. 40, no. 10, pp. 1619-1627, 2022.

[40] G. I. Waterhouse, J. B. Metson, H. Idriss, and D. Sun-Waterhouse, "Physical and optical properties of inverse opal CeO_2 photonic crystals," *Chemistry of materials,* vol. 20, no. 3, pp. 1183-1190, 2008.

[41] A. Panda, K. K. Das, K. R. Kaja, V. Gandi, S. G. Mohanty, and B. K. Panigrahi, "Low-cost high performance sustainable triboelectric nanogenerator based on laboratory waste," *Journal of Metals, Materials and Minerals,* vol. 35, no. 1, p. e2226, 2025.

[42] A. Panda, K. K. Das, K. R. Kaja, V. Gandi, S. G. Mohanty, and B. K. Panigrahi, "Single electrode mode triboelectric nano- generator for recognition of animal sounds," *Journal of Metals, Materials and Minerals,* vol. 34, no. 4, pp. 2170-2170, 2024.

[43] S. Nuthalapati, A. Chakraborthy, I. Arief, K. K. Meena, K. Ruthvik, R. R. Kumar, K. U. Kumar, A. Das, M. E. Altinsoy, A. Nag, "Wearable high-performance MWCNTs/PDMS nano-composite based triboelectric nanogenerators for haptic applications," *IEEE Journal on Flexible Electronics,* vol. 3, no. 9, pp. 393-400, 2024.

[44] O. Bazta, A. Urbieta, J. Piqueras, P. Fernandez, M.Addou, J. J. Calvino, and A. B. Hungria, "Influence of yttrium doping on the structural, morphological and optical properties of nano-structured ZnO thin films grown by spray pyrolysis," *Ceramics International,* vol. 45, no. 6, pp. 6842-6852, 2019.

[45] S. A. Behera, S. Panda, S. Hajra, K. R. Kaja, A. K. Pandey, A. Barranco, S. M. Jeong, V. Vivekananthan, H. J. Kim, and P. G. Achary, "Current trends on advancement in smart textile device engineering." *Advanced Sustainable Systems*, vol. 8 no. 12, p. 2400344, 2024.

[46] Y. Xu, L. Gao, and Z. Ding, "Synthesis and oxygen storage capacities of yttrium-doped CeO_2 with a cubic fluorite structure," *Materials,* vol. 15, no. 24, p. 8971, 2022.

[47] S. Iravani, "Green synthesis of metal nanoparticles using plants," *Green chemistry,* vol. 13, no. 10, pp. 2638-2650, 2011.

[48] O. V. Kharissova, H. R. Dias, B. I. Kharisov, B. O. Pérez, and V. M. J. Pérez, "The greener synthesis of nanoparticles," *Trends in biotechnology,* vol. 31, no. 4, pp. 240-248, 2013.

[49] J. Jalab, W. Abdelwahed, A. Kitaz, and R. Al-Kayali, "Green synthesis of silver nanoparticles using aqueous extract of Acacia cyanophylla and its antibacterial activity," *Heliyon,* vol. 7, no. 9, 2021.

[50] K. J. Rao, and S. Paria, "Aegle marmelos leaf extract and plant surfactants mediated green synthesis of Au and Ag nanoparticles by optimizing process parameters using Taguchi method," *ACS Sustainable Chemistry & Engineering,* vol. 3, no. 3, pp. 483-491, 2015.

[51] S. Muduli, and T. R. Sahoo, "Greener route for synthesis of cerium oxide and Fe-doped cerium oxide nanoparticles using a cacia concinna fruit extract," *International Journal of Materials Research,* vol. 114, no. 2, pp. 133-138, 2023.

[52] D. Toloman, A. Popa, R. B. Sonher, R. Bortnic, T. F. Marinca, I. Perhaita, M. R. Filip, and A. Mesaros, "Enhancing the photo-catalytic activity and luminescent properties of rare-earth-doped CeO_2 Nanoparticles," *Applied Sciences,* vol. 14, no. 2, p. 522, 2024.

[53] X. Xia, J. Li, C. Chen, L. Yuan-Pei, X. Mao, Z. Chu, D. Ning, J. Zhang, and F. Liu, "Collaborative influence of morphology tuning and RE (La, Y, and Sm) doping on photocatalytic performance of nanoceria," *Environmental Science and Pollution Research,* vol. 29, no. 59, pp. 88866-88881, 2022.